IEEE Access
Multidisciplinary | Rapid Review | Open Access Journal

Received March 20, 2019, accepted March 29, 2019, date of publication April 2, 2019, date of current version April 16, 2019.

Digital Object Identifier 10.1109/ACCESS.2019.2908830

Dual-Functional Coding Metasurfaces Made of Anisotropic All-Dielectric Resonators

LINDA SHAO[1], (Student Member, IEEE), MALIN PREMARATNE[2], (Senior Member, IEEE), AND WEIREN ZHU[1], (Senior Member, IEEE)

[1]Department of Electronic Engineering, Shanghai Jiao Tong University, Shanghai 200240, China
[2]Advanced Computing and Simulation Laboratory, Department of Electrical and Computer Systems Engineering, Monash University, Clayton, VIC 3800, Australia

Corresponding author: Weiren Zhu (weiren.zhu@sjtu.edu.cn)

This work was supported in part by the National Natural Science Foundation of China under Grant 61701303), in part by the Natural Science Foundation of Shanghai under Grant 17ZR1414300, and in part by the Shanghai Pujiang Program under 17PJ1404100.

ABSTRACT Digital coding metasurfaces, composed of only two types of unit cells with opposite phase responses (0 and π) that can map to the usual binary elements "0" and "1", are capable of generating coded pulsed sequences of electromagnetic waves. In this paper, we present a generic extensible strategy for designing dual-functional anisotropic coding metasurfaces based on all-dielectric resonators. The polarization-dependent beam manipulations are achieved via encoding the metasurfaces with different coding sequences in the two orthogonal polarizations of the electromagnetic wave propagating through the surface. As proof of concept, we show it is possible to achieve line focusing and point focusing in a single coding metasurface when illuminated by the x- or y-polarized electromagnetic waves. We also present anisotropic coding metasurfaces for realizing multi-beam generation and polarization-selected mirror/diffuse reflection. The near-field distributions and far-field scattering patterns extracted from full-wave simulations are presented to show the multiple functions of the metasurfaces and good conformance with theoretical predictions.

INDEX TERMS All-dielectric, anisotropic, coding metasurface, electromagnetic wave manipulation.

I. INTRODUCTION

Metamaterials made up from subwavelength building blocks have attracted enormous interest in recent years [1]–[3]. Due to their ability to tailor the permittivity and permeability beyond material composites found in nature, such metamaterials can be structured to manipulate electromagnetic waves in an unprecedented way. For example, many unusual electromagnetic properties not readily found in nature have been achieved by utilizing metamaterials, including invisibility cloaks [4], negative refraction material [5], and realization of perfect imaging [6]. In spite of these diverse functionalities of metamaterials, advances in the technological progress of metamaterial have been greatly limited because of bulky volumes, excess weight, and excessive intrinsic losses [7], [8]. Metasurfaces, the two-dimensional form of metamaterials, have ultrathin structures, low losses, and conformal capabilities, which could perfectly compensate the shortcomings of bulk metamaterials [9]–[11]. Particularly, metasurfaces have shown considerable potential for a wide range of applications, including perfect absorption [12], polarization control [13], beamforming [14], low scattering [15], vortex beam generation [16] and aberation-free flat lenses [17].

Recently, some quasi-continuous metasurfaces have been presented to further decrease the phase quantitative error [18]–[20]. Meanwhile, a concept of coding metasurfaces have been proposed to control electromagnetic waves, including anomalous beam reflection and diffuse scattering [21]. Two types of metasurface unit cells with 0 and π phase responses, representing '0' and '1' binary elements, respectively, are utilized for digital encoding there. For greater utility, pre-designing digital metasurfaces and programmable metasurfaces controlled by a field-programmable gate array is desired especially in applicating requiring functionalities, such as steering, bending, focusing and random electromagnetic wave scattering with the reasonable arrangements of the binary elements [21]–[23]. In addition, coding metasurfaces can also be controlled by varying the light intensity [24], [25]. Because of the isotropic geometries of the unit cells, the coding behaviors in such coding schemes are independent on the polarization status of the electromagnetic waves [26], [27]. Recently, digital anisotropic coding metamaterials have

The associate editor coordinating the review of this manuscript and approving it for publication was Shah Nawaz Burokur.

also been proposed [28]. The polarization control through anisotropic coding sequences are flexible and independent, and multiple functionalities can be realized via different polarizations. At radio frequencies, almost all coding metasurfaces are based on metallic subwavelength resonators. As an alternative, recent developments in high-permittivity dielectric materials suggest an alternative mechanism originated from Mie resonances [29]–[31], which shows the possibility of all-dielectric coding metasurfaces for the manipulation of electromagnetic waves. Compared to metallic resonator based metasurfaces, the use of dielectric resonators enables high efficiencies as they do not suffer from intrinsic nonradiative losses in metals.

In this letter, we present designs of dual-functional all-dielectric coding metasurfaces. The proposed all-dielectric unit cells can achieve 0 ('0' binary state) or π ('1' binary state) phase response under two orthogonal polarizations at 4 GHz. The manipulation of the reflected electromagnetic waves, including beam focusing, multi-beam generation, and diffuse scattering are achieved by all-dielectric metasurfaces with different coding arrays of '0' and '1' elements. We show that multiple functions supported by the anisotropic coding metasurfaces can be realized by altering the polarization directions of the incident wave. The simulated results agree well with theoretical predictions, substantiating the methodology and validity of the proposed design.

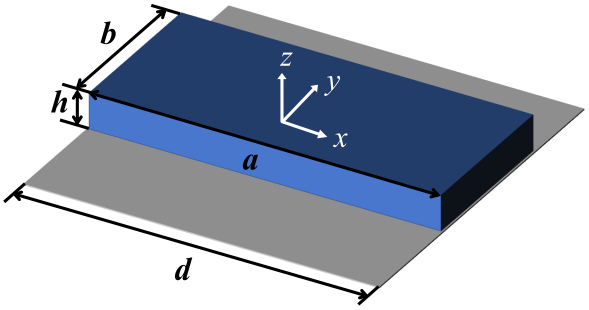

FIGURE 1. Geometry of the all-dieletric resonator.

II. UNIT CELL DESIGN

Fig. 1 shows a schematic of the unit cell of the metasurface, which is made out of an all-dielectric cubic block placed on a metallic ground. The dielectric material we chosen is a high-permittivity ceramic, $0.7Ba_{0.6}Sr_{0.4}TiO_3$-$0.3La(Mg_{0.5}Ti_{0.5})O_3$ (BST), which has a high dielectric constant ($\varepsilon_r = 110$) and a relatively low dielectric loss ($\tan\delta = 0.0015$). The thickness of the dielectric block is $h = 2$ mm and the period constant is $d = 20$ mm. The lengths of the dielectric block along the x and y directions are a and b, respectively. The metallic ground is assumed to be a perfect electric conductor. The anisotropic electromagnetic response of such a unit cell can be controlled by varying the side lengths a and b. The electromagnetic performance of the unit cells are studied via full-wave simulation using CST

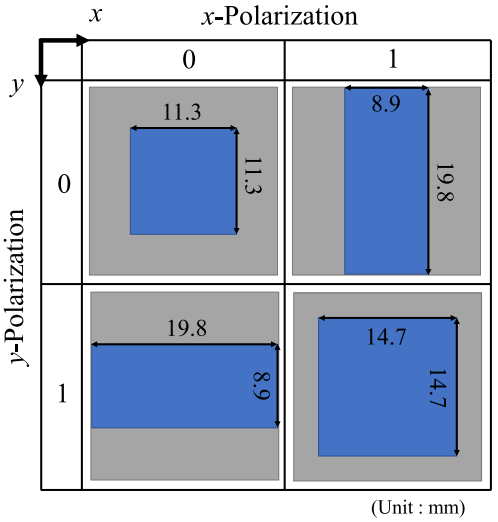

FIGURE 2. Top view of the 4 coding elements for the anisotropic metasurface.

Microwave studio. Periodic boundary conditions are applied along the x and y directions with perfectly matched layer boundary condition applied to the z direction.

In order to construct an anisotropic 1-bit dual-function metasurface for the x and y polarizations of the incident wave, it is necessary to have four unit cells that can generate the four coding elements, '0/0', '0/1', '1/0', and '1/1', where '0' and '1' refer to standard binary digits (i.e., 180° phase difference). Here, the elements '0/0' and '1/1' have isotropic responses whereas the remaining other two elements have anisotropic responses for the x and y polarizations. As the working frequency is set at 4 GHz, after parametric study, the geometrical parameters of the four unit cells are given in Fig. 2.

Figs. 3(a) and 3(b) show the reflection magnitudes and phases of the four unit cells under an x-polarized incident wave. Owing to the relatively low dielectric loss of the BST ceramic, the reflection magnitudes for all cases were kept relatively high values and are around 0.97 at 4 GHz. This clearly show that the all-dielectric digital coding metasurface will have high efficiency. In Fig.3(b), we see that the reflection phase curves for '0/0' and '0/1' show similar trends, while those for '1/0' and '1/1' are almost overlapped. Particularly, the reflection phases at 4 GHz are $\phi_{0/0} = \phi_{0/1} = 85°$ and $\phi_{1/0} = \phi_{1/1} = -95°$, the difference of which is exactly 180°. This implies that the change of the coding sequence along the y direction will not affect the performance of the metasurface for the x-polarized illumination. We can make use of this fact for designing polarization-dependent meta-mirror with dual functionalities. It is worth mentioning that the proposed four unit cells will have similar reflection responses under y-polarized illumination, since the unit cells for '0/1' and '1/0' are exactly the same but differs by a rotation angle of 90°. Therefore, by appropriately arranging the four coding elements '0/0', '0/1', '1/0', and '1/1', different digital

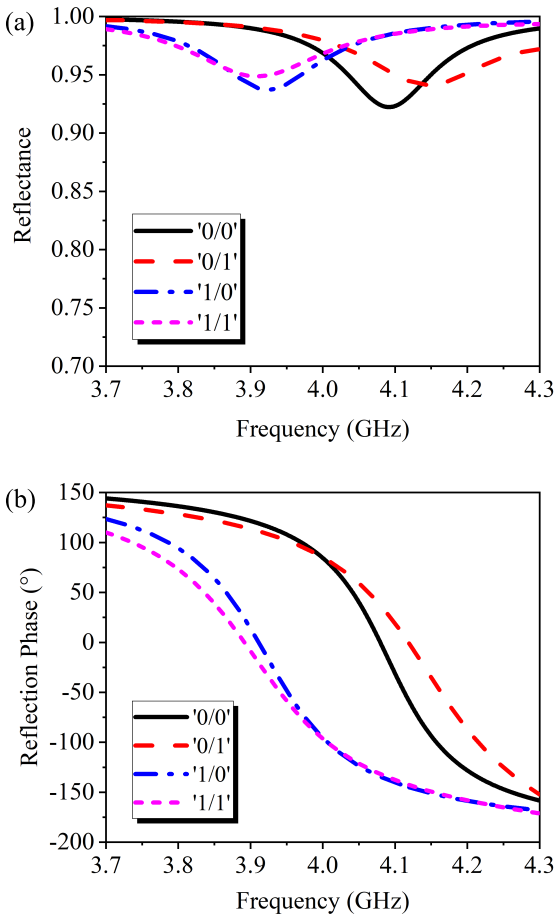

FIGURE 3. (a) Reflection magnitudes and (b) phases for the four coding elements under *x*-polarized incident wave.

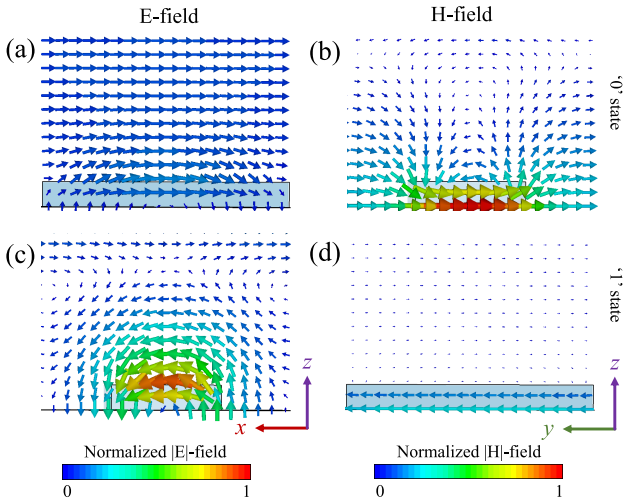

FIGURE 4. Electric and magnetic field distributions for the '0/1' unit cell at 4 GHz. (a) E-field in '0' state,(b) H-field in '0' state,(c) E-field in '1' state, and (d) H-field in '1' state.

coding sequences can be independently generated in both polarizations.

To further illustrate the scattering modes supported by the dielectric resonator, we analyzed the electric and magnetic field distributions in the '0/1' unit cell to show electromagnetic resonance behavior at the working frequency around 4 GHz. It is seen in Fig. 4 that a magnetic resonance is dominated for the '0' state while an electric resonance is found for the '1' state. Owing to this difference, the reflection phases of the two states show 180° difference.

III. DUAL-FUNCTIONAL CODING METAMATERIALS

A. THEORETICAL ANALYSIS

Assuming a metasurface consisting of $N \times N$ lattices, under normal incidence of the plane waves, the scattering phase of the (m, n)-th lattice φ_{mn} could be expressed as,

$$\varphi^x_{mn} = \alpha\pi, \tag{1a}$$
$$\varphi^y_{mn} = \beta\pi, \tag{1b}$$

where 'α/β' is the coding element of the (m, n)-th lattice with α and β being either 0 or 1.

It is worth noting that each unit cell as listed in Fig. 2 is designed assuming periodic boundary conditions. This implies that the coupling between unit cells is also considered during the design process. When designing a coding metasurface with different digital coding sequences, these coupling considerations are not automatically extended to account for coupling between adjacent unit cells as they are of different geometries. To minimize any extraneous effects arising due to such neglect of inter-coupling and boundary conditions, each lattice of the coding metasurface is assumed to be made of a sub-array $(M \times M)$ of identical unit cells. Therefore, the length of one square lattice is equal to $D = Md$.

1) FOCUSING PROPERTIES

A focal point will be obtained once an equal-phase wavefront is formed. The reflection phase of each unit cell should compensate the spatial phase delay due to the optical path difference between the distance from the focus point to the unit cell and focal length. The required phase shift of the reflection coefficient at the (m, n)-th lattice to achieve point focusing at $F(x_F, y_F, z_F)$ is:

$$\Delta\Phi_{mn} = k_0(\sqrt{(x_F - \xi_m)^2 + (y_F - \eta_n)^2 + z_F^2} - z_F) \tag{2}$$

where $k = 2\pi/\lambda$ is the wave vector in free space, $\xi_m = (m - 0.5)Md$ and $\eta_n = (n - 0.5)Md$ are the positional coordinates of the center of the (m, n)-th lattice.

Since the proposed unit cell only has two-phase states, the continuous phase shift should be quantized to:

$$\delta_{mn} = \begin{cases} 0, \Delta\Phi_{mn} \in [0 + 2n\pi, \quad \pi + 2n\pi), \\ \pi, \Delta\Phi_{mn} \in [\pi + 2n\pi, 2\pi + 2n\pi), \end{cases} \quad n \in Z. \tag{3}$$

When three-dimensional coordinate system degenerates into two-dimensional, the point-focused system will become a line-focused case.

2) SCATTERING PROPERTIES

The scattering pattern of the metasurface is given by:

$$f_u(\theta, \varphi) = f_{mn}(\theta, \varphi) \times \mathrm{AF}_u(\theta, \varphi), \tag{4}$$

where u represents the polarization of the metasurface, which could be x or y. $\mathrm{AF}_u(\theta, \varphi)$ is the array factor, $f_{mn}(\theta, \varphi)$ is the scattering pattern of the (m, n)-th lattice. θ and φ are the elevation and azimuth angles of an arbitrary direction, respectively. Since all the unit cells show nearly uniform reflectance, it is reasonable to assume $f_{mn}(\theta, \varphi)$ is fixed for all lattices. According to the planar array theory [32], $\mathrm{AF}_u(\theta, \varphi)$ can be written as:

$$\mathrm{AF}_u(\theta, \varphi) = \sum_{m=1}^{N}\sum_{n=1}^{N}(f^u_{i,mn} \times f^u_{r,mn} \times f^u_{p,mn}), \tag{5a}$$

$$f^u_{r,mn} = \exp(-j\varphi^u_{mn}), \tag{5b}$$

$$f^u_{p,mn} = \exp\left[-jk\sin\theta_u(\xi_m\cos\varphi_u + \eta_n\sin\varphi_u)\right]. \tag{5c}$$

Here, $f^u_{r,mn}$ and $f^u_{p,mn}$ are the phase components of each lattice attributed to reflection and position, respectively. Note that $f^u_{i,mn}$ is the phase component of the incident wave, which can be normalized as 1 for each lattice due to the use of plane wave in this work. Hence, according to scattering theory [33], the directivity function $\mathrm{Dir}_u(\theta, \varphi)$ of the metasurface, which shows the radiation energy concentrated in the direction of θ and φ, can be expressed as:

$$\mathrm{Dir}_u(\theta, \varphi) = \frac{4\pi\,|f_u(\theta, \varphi)|^2}{\int\int_{\theta,\phi}|f_u(\theta, \varphi)|^2\sin\theta_u \mathrm{d}\theta_u \mathrm{d}\varphi_u}. \tag{6}$$

According to the above equation, the scattered fields can be controlled through the coding sequences of the metasurface lattices. For example, when the periodic coding sequence is 010101.../010101..., the normally incident beam will predominantly be reflected into two symmetrically oriented directions with $\varphi_1 = 90°$ and 270°, and $\theta_1 = \arcsin(\lambda/2D)$. For the periodic coding sequence of 010101.../101010.../010101.../101010..., the normally incident beam will mainly be reflected to four symmetrically oriented directions with $\varphi_2 = 45°$, 135°, 225°, 315°, and $\theta_2 = \arcsin(\lambda/\sqrt{2}D)$.

When the local reflection phases of coding unit cells are randomly distributed, the metasurface can be used for reducing the scattering of the electromagnetic waves by redirecting electromagnetic energies to all directions. Compared to a metallic plate with the same size, the RCS reduction (RCSR) caused by the coding metasurface is

$$\mathrm{RCSR} = \frac{\lambda^2}{4\pi N^2 M^2 d^2}\max_{\theta,\varphi}\{[\mathrm{Dir_u}(\theta, \varphi)]\}, \tag{7}$$

where λ is the free space wavelength. The best RCS reduction can be achieved through optimizing the distribution of '0' and '1' lattices on coding metasurfaces.

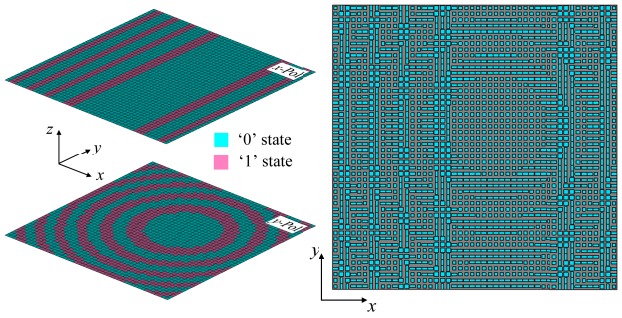

FIGURE 5. Illustration of the design of the anisotropic coding metasurface encoded with coding array G_1.

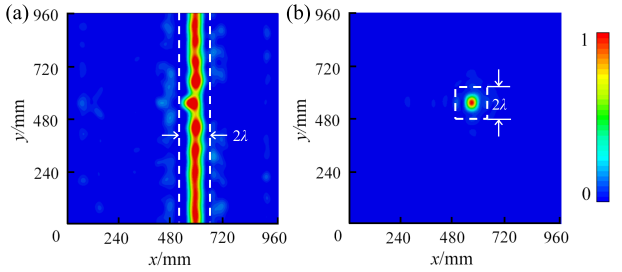

FIGURE 6. Normalized electric field intensity distribution at the plane $z = 375$ mm for the metasurface (coding array G_1) under (a) x-polarized or (b) y-polarized incident wave.

B. DESIGN OF ANISOTROPIC ALL-DIELECTRIC CODING METASURFACES

As a first example, an anisotropic metasurface is designed for beam focusing when illuminated by a normally incident plane wave. We encode a metasurface with rings of '0' and '1' binary elements to achieve point focusing and lines of '0' and '1' binary elements to achieve line focusing under x- and y-polarization, respectively. By combining those two isotropic coding arrays, the anisotropic metasurface with corresponding quantized coding array G_1 is built up, as depicted in Fig. 5. The metasurface includes 48 × 48 unit cells. Here, the entire encoded metasurface is numerically studied in CST Microwave Studio, where open boundary conditions are applied to the four lateral sizes of the metasurface. Under an x-polarized excitation at 4 GHz, a well-defined focusing line $x = 580$ mm is clearly observed, as shown in Fig. 6(a). Meanwhile, Fig. 6(b) presents a focusing point (551 mm, 551 mm) when the metasurface is under a y-polarized excitation. The normalized electric field intensity results provide with us the decisive evidence for the powerful focusing capability of the metasurface.

In addition, under x- and y–polarized incidences, the focusing efficiencies, defined as the ratio of the reflected power in the focusing regions (marked in Fig. 6) to the incident power, are 29.75% and 18.86%, respectively. Even through the reflectance of the all-dielectric unit cell is nearly uniform (over 97%), the quantitative phase level ('0' and 'π') limits the focusing performance, which results relatively low focusing efficiencies. Such an issue could be overcome

by employ continuous phase variation in the design of metasurfaces.

Besides, we encode a metasurface with a coding sequence of '010101.../010101...' along the x direction and a coding sequence of '010101.../101010...' along the y direction. Then, the coding array G_2 can be formed by repeating a coding matrix,

$$\begin{pmatrix} 0/1 & 1/0 \\ 0/0 & 1/1 \end{pmatrix}.$$

Here, each lattice is composed of 4×4 unit cells ($M = 4$). With such coding sequences, the metasurface is able to reflect the x-polarized (or y-polarized) incident planar wave into two (or four) beams, as per the derivation in (4). The elevation angles of reflection can be calculated as $\theta_x = \arcsin(\lambda/2D) = 28.0°$ and $\theta_y = \arcsin(\lambda/\sqrt{2}D) = 41.5°$ under x- and y-polarizations, respectively.

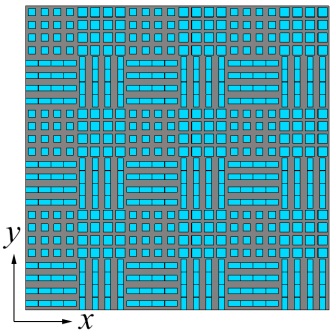

FIGURE 7. Metasurface encoded with coding array G_2.

The encoded metasurface with coding array G_2 includes 6×6 lattices, as illustrated in Fig. 7. Under a plane wave excitation, the three-dimensional (3D) far-field scattering patterns of the anisotropic coding metasurface are shown in Figs. 8(a) and 8(b) at $f = 4$ GHz. It is seen that, for the x-polarized case, most of the incident electromagnetic energy is deflected to two symmetrically oriented directions in the plane parallel to the polarization directions. While for the y-polarized case, the incident beam is deflected to four symmetrically oriented beams with 45° with respect to xoz and yoz planes. The elevation angles for these two cases are $\theta_x = 27.0°$ and $\theta_x = 39.2°$, which matches very well with the theoretical expectation. The slight disturbance observed in the scattered electric field to the real reflection phases is attributed to adjacent lattice coupling, which makes the reflection phases of the binary elements are not exactly 0 or π at 4 GHz. However, this effect can be suppressed if the size of each lattice contains more identical elements.

When the normally incident electromagnetic beam has a polarization angle of 45° (with respect to the x axis), it will split into six beams, as shown in Fig. 8(c). This is because that the incident beam has both polarization components, where two reflected beams are contributed to the x component while another four beam are contributed to the y component of the incident beam. It is worth noting that the intensities

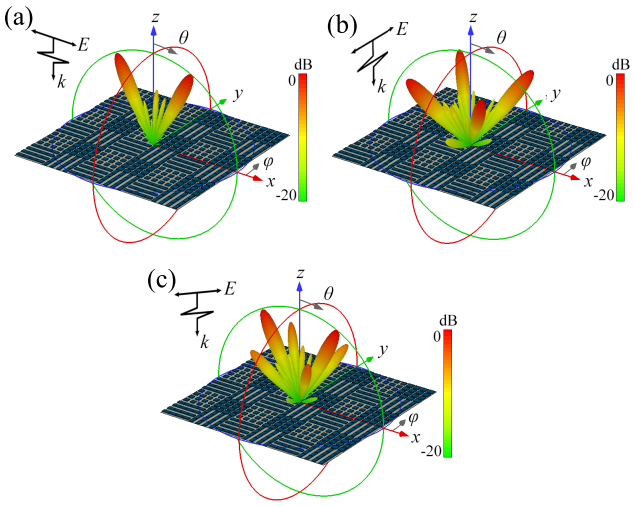

FIGURE 8. 3D far-field scattering patterns of metasurface under incident waves with polarizations along (a) x axis, (b) y axis, and (c) 45° with respect to x axis.

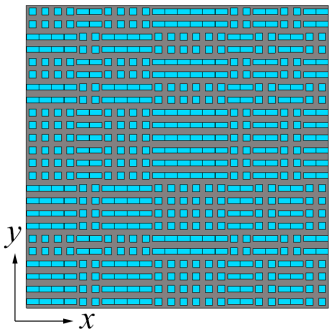

FIGURE 9. Metasurface encoded with coding arrays G_3.

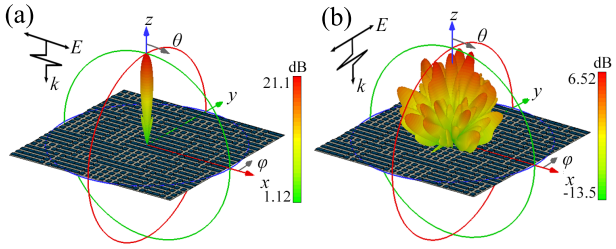

FIGURE 10. 3D far-field scattering patterns of metasurface under incident waves with polarizations along (a) x axis and (b) y axis, respectively.

of these beams can be arbitrarily controlled by adjusting the polarization angle of the incident beam. Such a digital coding metasurface can be used as a multi-beam generator or a tunable beam splitter.

The anisotropic all-dielectric digital coding metasurface can also be designed for mirror reflection for the x-polarized beam (with all units on '0' state) and diffuse reflection for the y-polarized beam (with a randomly generated coding sequence), depicted as the coding arrays G_3 in Fig. 9. In such a case, the normally incident x-polarized beam is perfectly

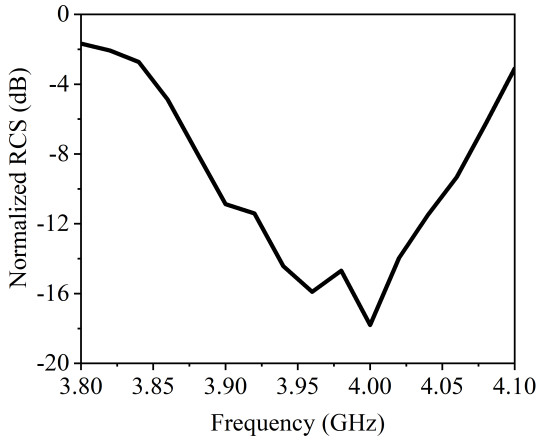

FIGURE 11. Simulated monostatic RCS reductions curves of the metasurface under *y*-polarized normal incidence.

reflected back, as shown in Fig. 10(a). However, for the *y*-polarization, the scattered fields are very much suppressed in all directions, as observed in Fig. 10(b). This confirms the significant reduction of monostatic RCS from the metasurface. The diffuse scattering is caused by the destructive inference resulting from the random phase distributions of the unit cells, and indicates that the scattering of a metallic plate can be significantly reduced by covering these encoded metasurfaces. To characterize the scattering reduction performance, we show the monostatic RCS obtained by full-wave simulation, as shown in Fig. 11. Compared to a metallic plate of equivalent size to that of the metasurface, an RCS reduction of at least 10 dB is guaranteed within the frequency band of 3.90 – 4.05 GHz and the peak value of RCS reduction is over 18 dB through the coding metasurface with coding array G_3.

IV. CONCLUSION

In summary, we have presented a generic scheme for the design of dual-functional anisotropic digital coding metasurfaces using all-dielectric resonator building blocks. To illustrate the versatility of our scheme, we showcased three metasurfaces with various digital coding arrays that utilized both polarizations. The beam focusing, beam splitting, and diffuse scattering features were demonstrated via different digital coding arrays and the results indicate that these metasurfaces exhibit polarization-dependent multiple functionalities. Numerical simulations of the near field results and far field scattering patterns confirmed the multiple functionalities of the proposed metasurfaces. The proposed digital anisotropic coding metasurface may find useful in multi-beam generation, tunable beam splitting, flexible beam focusing and RCS reduction.

REFERENCES

[1] V. G. Veselago and E. E. Narimanov, "The left hand of brightness: Past, present and future of negative index materials," *Nature Mater.*, vol. 5, no. 10, p. 759, Oct. 2006.

[2] F. Zhou *et al.*, "Hiding a realistic object using a broadband terahertz invisibility cloak," *Sci. Rep.*, vol. 1, p. 78, Sep. 2011.

[3] L. I. Basilio, L. K. Warne, W. L. Langston, W. A. Johnson, and M. B. Sinclair, "Microwave-frequency, negative-index metamaterial designs based on degenerate dielectric resonators," *IEEE Antennas Wireless Propag. Lett.*, vol. 11, pp. 113–116, 2012.

[4] D. Schurig *et al.*, "Metamaterial electromagnetic cloak at microwave frequencies," *Science*, vol. 314, no. 5801, pp. 977–980, Oct. 2006.

[5] H. Shin and S. Fan, "All-angle negative refraction for surface plasmon waves using a metal-dielectric-metal structure," *Phys. Rev. Lett.*, vol. 96, Feb. 2006, Art. no. 073907.

[6] J. B. Pendry, "Negative refraction makes a perfect lens," *Phys. Rev. Lett.*, vol. 85, no. 18, pp. 3966–3969, Oct. 2000.

[7] R. Liu, C. Ji, J. J. Mock, J. Y. Chin, T. J. Cui, and D. R. Smith, "Broadband ground-plane cloak," *Science*, vol. 323, no. 5912, pp. 366–369, Jan. 2009.

[8] T. Ergin, N. Stenger, P. Brenner, J. B. Pendry, and M. Wegener, "Three-dimensional invisibility cloak at optical wavelengths," *Science*, vol. 328, no. 5976, pp. 337–339, Apr. 2010.

[9] C. Pfeiffer and A. Grbic, "Metamaterial huygens' surfaces: Tailoring wave fronts with reflectionless sheets," *Phys. Rev. Lett.*, vol. 110, May 2013, Art. no. 197401.

[10] M. Kang, W. Zhu, and I. D. Rukhlenko, "Experimental observation of the topological structure of exceptional points in an ultrathin hybridized metamaterial," *Phys. Rev. A, Gen. Phys.*, vol. 96, Dec. 2017, Art. no. 063823.

[11] M. R. Akram, M. Q. Mehmood, T. Tauqeer, A. S. Rana, I. D. Rukhlenko, and W. Zhu, "Highly efficient generation of bessel beams with polarization insensitive metasurfaces," *Opt. Express*, vol. 27, no. 7, pp. 9467–9480, Apr. 2019.

[12] S. Liu, H. B. Chen, and T. J. Cui, "A broadband terahertz absorber using multi-layer stacked bars," *Appl. Phys. Lett.*, vol. 106, no. 15, Apr. 2015, Art. no. 151601.

[13] C. Pfeiffer and A. Grbica, "Cascaded metasurfaces for complete phase and polarization control," *Appl. Phys. Lett.*, vol. 102, no. 23, 2013, Art. no. 231116.

[14] J. Li *et al.*, "Design of a broadband metasurface luneburg lens for full-angle operation," *IEEE Trans. Antennas Propag.*, to be published. doi: 10.1109/TAP.2018.2889006.

[15] Y. Zhuang, G. Wang, Q. Zhang, and C. Zhou, "Low-scattering tri-band metasurface using combination of diffusion, absorption and cancellation," *IEEE Access*, vol. 6, pp. 17306–17312, 2018.

[16] M. R. Akram, X. Bai, R. Jin, G. A. E.Vandenbosch, M. Premaratne, and W. Zhu, "Photon spin hall effect based ultra-thin transmissive metasurface for efficient generation of OAM waves," *IEEE Trans. Antennas Propag.*, to be published. doi: 10.1109/TAP.2019.2905777.

[17] D. Lin, P. Fan, E. Hasman, and M. L. Brongersma, "Dielectric gradient metasurface optical elements," *Science*, vol. 345, no. 6194, pp. 298–302, 2014.

[18] M. Pu *et al.*, "Catenary optics for achromatic generation of perfect optical angular momentum," *Sci. Adv.*, vol. 1, no. 9, 2015, Art. no. e1500396. [Online]. Available: http://advances.sciencemag.org/content/1/9/e1500396

[19] Y. Guo *et al.*, "Merging geometric phase and plasmon retardation phase in continuously shaped metasurfaces for arbitrary orbital angular momentum generation," *ACS Photon.*, vol. 3, no. 11, pp. 2022–2029, Nov. 2016.

[20] Y. Guo, X. Ma, M. Pu, X. Li, Z. Zhao, and X. Luo, "High-efficiency and wide-angle beam steering based on catenary optical fields in ultrathin metalens," *Adv. Opt. Mater.*, vol. 6, no. 19, p. 1800592, Jul. 2018.

[21] T. J. Cui, M. Q. Qi, X. Wan, J. Zhao, and Q. Cheng, "Coding metamaterials, digital metamaterials and programmable metamaterials," *Light Sci. Appl.*, vol. 3, no. 10, p. e218, Oct. 2014.

[22] X. Liu, J. Gao, L. Xu, X. Cao, Y. Zhao, and S. Li, "A coding diffuse metasurface for RCS reduction," *IEEE Antennas Wireless Propag. Lett.*, vol. 16, pp. 724–727, 2016.

[23] T. J. Cui, "Microwave metamaterials-from passive to digital and programmable controls of electromagnetic waves," *J. Opt.*, vol. 19, no. 8, Jul. 2017, Art. no. 084004.

[24] X. G. Zhang *et al.*, "Light-controllable digital coding metasurfaces," *Adv. Sci.*, vol. 5, no. 11, 2018, Art. no. 1801028.

[25] X. G. Zhang, W. X. Jiang, and T. J. Cui, "Frequency-dependent transmission-type digital coding metasurface controlled by light intensity," *Appl. Phys. Lett*, vol. 113, no. 9, 2018, Art. no. 091601.

[26] L.-H. Gao *et al.*, "Broadband diffusion of terahertz waves by multi-bit coding metasurfaces," *Light Sci. Appl.*, vol. 4, no. 9, p. e324, Sep. 2015.

[27] L. Liang *et al.*, "Metamaterials: Anomalous terahertz reflection and scattering by flexible and conformal coding metamaterials," *Adv. Opt. Mater.*, vol. 3, no. 10, p. 1373, 2015.
[28] S. Liu *et al.*, "Anisotropic coding metamaterials and their powerful manipulation of differently polarized terahertz waves," *Light Sci. Appl.*, vol. 5, no. 5, May 2016, Art. no. e16076.
[29] Q. Zhao, J. Zhou, F. Zhang, and D. Lippens, "Mie resonance-based dielectric metamaterials," *Mater. Today*, vol. 12, no. 12, pp. 60–69, Dec. 2009.
[30] L. Shao, W. Zhu, X. Liang, J. Geng, and R. Jin, "Anomalous refraction in an all-dielectric gradient metasurface," in *Proc. IEEE 6th Asia-Pacific Conf. Antennas Propag. (APCAP)*, Oct. 2017, pp. 1–3.
[31] W. Zhu, F. Xiao, M. Kang, and M. Premaratne, "Coherent perfect absorption in an all-dielectric metasurface," *Appl. Phys. Lett.*, vol. 108, Mar. 2016, Art. no. 121901.
[32] E. F. Knott, *Antenna Theory and Design*. Hoboken, NJ, USA: Wiley, 2005.
[33] E. F. Knott, J. F. Shaeffer, and M. T. Tuley, *Radar Cross Section*, 2nd ed. Raleigh, NC, USA: SciTech Publishing, 2004.

LINDA SHAO was born in 1995. She received the B.S. degree in electrical engineering and its automation from Center South University, Changsha, Hunan, in 2017. She is currently pursuing the Ph.D. degree in electronic engineering with Shanghai Jiao Tong University, Shanghai. Her current research interest includes electromagnetic properties of all-dielectric metasurfaces.

MALIN PREMARATNE (S'95–M'98–SM'03) received the B.Sc. degree in mathematics, the B.E. degree (Hons.) in electrical and electronics engineering, and the Ph.D. degree from The University of Melbourne, in 1995, 1995, and 1998, respectively.

From 1998 to 2000, he was with the Photonics Research Laboratory, The University of Melbourne, where he was the Co-Project Leader of the CRC Optical Amplifier Project and was also associated with Telstra, Australia, and Hewlett Packard, USA. From 2001 to 2003, he was a consultant to several companies, including Cisco, Lucent Technologies, Ericsson, Siemens, VPI Systems, Telcordia Technologies, Ciena, and Tellium. Since 2004, he has been guiding the research program in high-performance computing applications to complex systems simulations at the Advanced Computing and Simulation Laboratory, Monash University, Clayton, where he is currently the Vice President of the Academic Board Monash University and a Full Professor. He is also a Visiting Researcher with the Jet Propulsion Laboratory, Caltech, The University of Melbourne, The Australian National University, the University of California at Los Angeles, the University of Rochester New York, and Oxford University. He has authored more than 200 journal papers and one book. He has given presentations on modeling and simulation of optical devices at many major international meetings and scientific institutions in USA, Europe, Asia, and Australia.

Dr. Premaratne is a Fellow of the Optical Society of America and a Fellow of the Institute of Engineers Australia. He is currently an Associate Editor of the IEEE Photonics Technology Letters, the IEEE Photonics Journal, and *OSA Advances in Optics and Photonics*.

WEIREN ZHU (M'16–SM'18) received the B.S. and Ph.D. degrees in physics from Northwestern Polytechnical University, Xi'an, China, in 2006 and 2011, respectively.

From 2011 to 2012, he was a Postdoctoral Fellow with the Nonlinear Physics Centre, The Australian National University, Canberra, ACT, Australia. From 2012 to 2016, he was a Research Fellow with the Advanced Computing and Simulation Laboratory (AχL), Department of Electrical and Computer Systems Engineering, Monash University, Clayton, VIC, Australia. Since 2016, he has been with the Department of Electronic Engineering, Shanghai Jiao Tong University, Shanghai, China, as an Associate Professor. He has authored or coauthored more than 100 refereed journal papers and more than 40 conference proceedings. His current research interests include electromagnetic metamaterials, antennas and RF devices, and surface plasmon polaritons.

Dr. Zhu is a Senior Member of the Optical Society of America. He was a recipient of the Shanghai Pujiang Talent Program by Shanghai Science and Technology Commission, in 2017. He is currently serving as an Associate Editor for the IEEE Photonics Journal and an Associate Editor for the IEEE Access.